Additive Manufacturing of Thermosetting Resins via Direct Ink Writing and Radio-Frequency Heating and Curing

Anubhav Sarmah[a,1], Suchi K. Desai[a,1], Ava G. Crowley[a], Gabriel C. Zolton[a], Guler Bengusu Tezel[a,b], Ethan M. Harkin[a], Thang Q. Tran[a,c], Kailash Arole[d], Micah J. Green[a,d,*]

[a] Artie McFerrin Department of Chemical Engineering, Texas A&M University, College Station, TX, 77843, USA

[b] Chemical Engineering Department, Bolu Abant Izzet Baysal University, Bolu, 14030, Turkey

[c] Singapore Institute of Manufacturing Technology, 73 Nanyang Drive, 637662, Singapore

[d] Department of Materials Science and Engineering, Texas A&M University, College Station, TX, 77843, USA

Abstract

Direct Ink Writing (DIW) is an extrusion-based additive manufacturing method where the print medium is a liquid-phase 'ink' dispensed out of small nozzles and deposited along digitally defined paths. Conventional DIW methods for thermosetting resins rely on the use of viscosity modifying agents, novel crosslinking chemistries, and/or long curing schedules in an oven. Here we demonstrate the use of a co-planar radio frequency applicator to generate an electric field, which can be used to rapidly heat and cure nano-filled composite resins as they are printed. This method avoids the need for an oven or post- curing step. This process consists of a sequential print-and-cure cycle which allows for printing of high-resolution, multi-layered structures. Every extruded layer is partially cured using RF before depositing the next layer; this allows the printed part to maintain structural integrity without buckling under its own weight. The process enables both increased throughput and decreased touch time relative to traditional part manufacturing. Commercial epoxy resin with varied nano-filler loadings were examined as DIW candidates. Rheological characterization was used to assess both curing kinetics and printing behavior. After printing, the thermo-mechanical properties, surface finish, and shape retention of RF-cured samples were evaluated and found to be comparable against samples conventionally cured in an oven. This method of manufacturing establishes RF heating as a suitable alternative to conventional methods, facilitating rapid, free-form processing of thermosetting resins without a mold.

Keywords: Direct Ink Writing, Radio Frequency Heating, Thermosetting Resin, Free-Form Processing

[1]: These authors contributed equally to the manuscript.

[*]: Corresponding author: E-mail: micah.green@tamu.edu (Micah J. Green)

Introduction

Thermosetting polymers form crosslinked networks when heated and cured. Epoxies are a very commonly used type of crosslinkable thermosets; such crosslinked networks feature high mechanical strength, resistance to chemical degradation, and thermal stability. These properties make thermosets, including epoxies, a popular choice for applications ranging from battery frameworks to aerospace and automotive structures[1]. Conventional methods of manufacturing parts from thermosetting polymers involve the use of molds to cure resin matrices in high-temperature ovens. This process is energy consuming, labor intensive, and slow; moreover, there are limitations on achievable part geometries due to the requirement of part-specific molds[2, 3].

Additive manufacturing avoids many of the downsides of conventional manufacturing methods and allows faster on-demand, and energy efficient production of complex structures with custom geometries[4]. Additive manufacturing has previously been explored to 3D print thermoplastics[5-7] and metals[8-10]. The development of an on-demand, rapid production technique for thermosetting polymers could facilitate distributed manufacturing by setting up industries near the end user[11].

Previous studies for additive manufacturing of crosslinkable resins using direct-ink write (DIW) printing have largely been limited to photocurable materials[12-16]. This 3D printing method can also be applied to print dual-cure resins; in such cases, thermosets are combined with photocurable materials, resulting in a resin that is both light and chemically activated[17, 18]. However, methods that use dual-cure require changes to the resin chemistry to make the material UV curable; this alteration to resin chemistry limits the use of photocurable resins for industrial applications. Additive manufacturing of thermosets via frontal polymerization (FROMP) has also been studied to print complex shapes; this involves the production of a propagating reaction wave that allows for rapid cross-linking of the initial monomer. However, this method is restricted by the limited number of resin chemistries that can be printed[19-21].

The primary challenge with the use of DIW printing for manufacturing thermoset parts is ensuring shape retention during the printing and curing processes. Some studies use a thixotropic support bath to ensure shape retention of the thermosetting resin.[22] The resin is injected or printed directly in a support bath, and the structure is then partially cured at room temperature. The structure is then removed from the support bath and cured completely in an oven. The use of such a bath for DIW printing requires long oven curing schedules at low temperatures to prevent the printed structure from collapsing during the curing process.

The use of viscosifiers has also been investigated to increase the yield stress and load bearing capacity of the resin for DIW printing[23, 24]. A higher viscosity improves shape retention during the printing process which enables the production of high-resolution structures with multiple layers in the z-direction;[25] however, a higher viscosity also increases the yield stress of the resin and makes the ink difficult to print using commercially available 3D printers. Additionally, the viscosity of these inks drastically decreases upon heating prior to crosslinking. Thus, when using a high viscosity resin for DIW printing, the printed structures need to be cured at low temperatures for an extended period of time (24+ hours)[26, 27] to maintain the resolution of the printed structure.

Recently, our group has shown that carbon nanomaterials heat up rapidly in response to radio frequency (RF) fields [5, 7, 28-33], i.e., electromagnetic fields with a frequency within the range of 20 kHz to 300 GHz. RF susceptor materials include graphite, graphene oxide, laser-induced graphene, carbon black, and carbon fibers. Susceptor materials can be used as fillers in thermosetting matrices, allowing for rapid heating and curing of the nano-filled resin upon application of an RF field. RF heating offers several benefits like volumetric and targeted heating. Bulk specimens with RF susceptors can be heated volumetrically using RF fields; this method eliminates the need for large ovens to heat and cure the specimens. Some processes, like bonding, require site-specific heating, which become possible using RF fields. Targeted

heating avoids the need to heat the entire structure, which can introduce residual thermal stresses in the assembly after cooling[34]. RF heating has shown potential to reduce fabrication time and provide an energy efficient alternative for numerous applications where targeted and volumetric heating are needed such as inter-layer adhesion in 3D printed thermoplastics[5], bonding thermoplastic surfaces together[32], curing pre-ceramic polymer composites[31], reduction of graphene oxide[29], and processing of thermosetting prepregs[33]. Compared to traditional heating and processing methods, RF heating provides faster heating rates with lower infrastructure requirements and better energy efficiency; non-contact RF applicators or capacitors can be used for out-of-oven processing, allowing for distributed manufacturing.

In our previous work, we demonstrated that multi-layered structures can be produced using RF heating and selective curing of carbon nanotube (CNT)-filled thermosetting epoxies.[35] An RF applicator was moved relative to a reservoir of CNT-filled resin, thus, heating and curing the resin exposed to the RF field. We demonstrated the benefits of RF heating in additive manufacturing of thermosetting resins over conventional curing methods; however, in the previous method, the resolution of the printed structure was limited by heat diffusion in the resin reservoir, thus leading to rough edges and surface finish on the final part.

In this study, we demonstrate a new process involving a layer-by-layer, print and cure cycle for additive manufacturing of high-resolution, multi-layered structures. Here, each layer printed using a conventional DIW printer is partially cured using RF heating before a new layer is deposited. This print and cure cycle allows the printed structure to maintain its integrity and support itself without collapsing as subsequent layers are printed (**Figure 1**). We examine commercial epoxy resin with varied CNT loadings as DIW candidates; we use rheological characterization to assess curing kinetics and printing behavior, and investigate response to RF fields to assess RF heating properties of the candidate resins. We also model the spatiotemporal kinetics of our printing and curing process, and create complex 3D structures in our simulations. This work facilitates rapid, free-form processing of commercial thermosets which establishes RF heating combined with DIW printing as a promising method for additive manufacturing of thermosetting systems with reduced processing time and energy requirements.

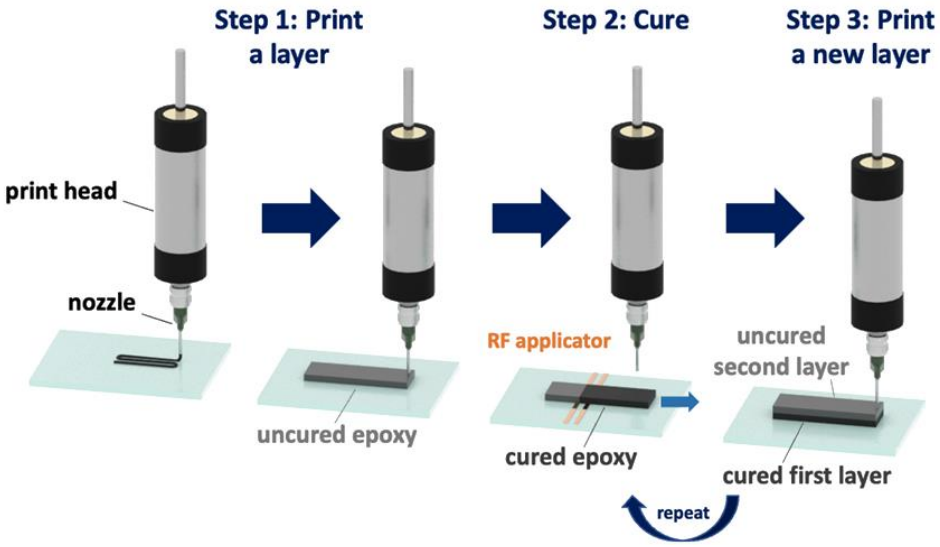

Figure 1: Schematic representing the direct-ink write printing process using radio-frequency assisted heating and curing. Step 1 represents the DIW printing process; step 2 demonstrates the RF heating and partial curing process; and step 3: shows the deposition of a new printed layer, after which the print-and-cure cycle is repeated.

Experimental Methods

Materials

Bisphenol A diglycidyl ether (DGEBA) epoxide (Hexion, Columbus, OH) was heated at 60 °C in an oven to melt crystallized material. Before mixing, the resin was allowed to cool at room temperature. Jeffamine T403 polyetheramine (Huntsman, The Woodlands, TX) was used as a low viscosity hardener. The epoxide and curing agent were combined in a weight ratio of 100:49. Multi-walled carbon nanotubes (MWCNTs) (cheaptubes, Cambridgeport, VT) were added to the resin at various loadings between 3-7 wt.%. To ensure uniform dispersion, the MWCNTs were mixed into the resin using a planetary mixer for 10 minutes. Following this, the mixture was degassed for 20 minutes in a vacuum oven.

Rheology

Rheological measurements were carried out using a stress-controlled rheometer (Anton Paar, MCR 301) at room temperature (at ~23 °C) with a 25 mm diameter stainless steel top fixture and a 50 mm disposable aluminum plate bottom fixture with a gap of 0.1 mm. Rheological properties of uncured candidate resins were evaluated prior to printing. An oscillatory amplitude sweep at constant temperature (25 ˚C) and frequency (1 Hz) was used to determine the linear viscoelastic region for each candidate resin. The acceptable region for linear viscoelasticity was in the range of 0.01-0.5% for each of the samples. In further tests, a constant strain of 0.3% was used. The amplitude sweep also was used to determine the yield stress of the uncured resin at each loading. A frequency sweep test was used to observe the storage (G') and loss (G'') modulus as a function of frequency before the candidate resin is exposed to high shear. A three-step steady-shear thixotropy test was conducted to mimic extrusion from the print head and determine time-dependent recovery behavior of candidate resins. There are three regions in this test: an initial rest period (0.01 s^{-1}), a high shear-rate step (1000 s^{-1}), and the recovery period (0.01 s^{-1}). After this, another frequency sweep test was conducted on each candidate resin to observe changes in storage (G') and loss (G'') modulus as a function of frequency after high shear.

Radio Frequency setup and Heating Response

A stationary, co-planar radio frequency (RF) applicator was fabricated by laser-etching copper traces on an FR4 substrate. RF waves were generated using a RIGOL DSG15 signal generator and amplified using a PRANA GN 500 amplifier. The RF waves, supplied to the applicator using a coaxial cable, created an electric field that extends above the plane to heat nano-filled resin composites. Maximum heating rate for each candidate resin was determined. For this test, constant RF power at 1 W was supplied to samples with an approximate thickness of 2 mm (electric field weakens in the z-direction). Maximum temperature was recorded using a thermal camera (FLIR Systems, Inc., A655sc) placed above the sample (**Figure S1**). For each candidate resin, a sample undergoes a cycle of heating for 1 second followed by a 13 second rest period for every integer frequency value between 1-200 MHz. For each heating cycle, heating rate was calculated using data points taken prior to heating and data points taken once the temperature had reached a maximum.

Printing and Curing

The HyRel Engine Standard Resolution direct ink writing printer was used for printing experiments. The prepared sample was loaded into a 15-cc dual-gasket stainless cartridge for a HyRel EMO-XT print head (Hyrel 3D; Norcross, GA) with nozzles of sizes 0.6-0.84 mm (from Structur3D)

attached to the print head. For each printed structure, the CAD files were created using Solidworks, and converted into g-codes using Hyrel's Repetrel software in conjunction with Slic3r.

After each layer was printed, the sample was transferred to the RF applicator and partially cured at ~150 °C for 45-60 seconds. The target temperature of ~150 °C was maintained by manually modulating the RF power. This print-and-cure cycle was repeated for each layer (**Figure 1**). The final structure was cured completely at ~150 °C for 10 minutes after the last layer was printed.

Simulations

The model described below was discretized using the finite difference method and solved using a built-in implicit solver (with a mass matrix) in MATLAB R2021b. The simulations are two dimensional (x-z) and the thickness of the printed structure is assumed to be negligible in the y-direction. The spatiotemporal kinetics are described by two ordinary differential equations. The modified Kamal-Sourour equation was used to model the reaction kinetics[35, 36] (**Equation 1**).

$$\frac{dX}{dt} = (kX^m)(1-X)^n \qquad (1)$$

Here, *dX/dt* is the curing rate, *X* is the degree of cure, *k* is the temperature-dependent reaction rate constant, and *m* and *n* are empirical reaction constants that reflect reaction orders and define the initiation and propagation stages of curing, respectively. The parameters in **Equation 1** (*k*, *m*, and *n*), were determined using DSC experiments in the temperature range of 80-110 °C. The data collected from these experiments was fitted to the modified Kamal-Sourour equation, and the activation energy was calculated to be ~33 kJ/mol using the Arrhenius equation. The calculated activation energy was used in the model to compute *k* as a function of local temperature.

The energy balance for the model is as shown in **Equation 2**:

$$\frac{dT}{dt} = \alpha\nabla^2 T + Q_{ext} + \frac{\Delta H_{rxn}}{C_p} + Q_{RF}(x,z) \qquad (2)$$

Here, *dT/dt* is the rate of change in temperature, the $\nabla^2 T$ term indicates heat conduction within the resin, and the ΔH_{rxn} term accounts for the heat generated by the exothermic curing reaction. Material functions like the thermal diffusivity (α) and the heat capacity (C_p) are matched to the epoxy resin itself.

The thermal transport in the y direction is described by the Q_{ext} term, which includes the heat losses to surroundings via convection to the air through the front and back of the sample (**Figure S2**). These are written as shown in **Equation 3**:

$$Q_{ext} = 2 \times \left[\frac{h}{\rho\, C_p t_{resin}}\,(T - T_{air})\right] \qquad (3)$$

Here, *h* is the convection coefficient for air (~30 W/(m^2 K)), ρ is the density of the resin (900 kg/m^3), C_p is the heat capacity of the resin (~2000 J/(kg · K)), t_{resin} is the height of the resin in the reservoir (1 mm), *T* is the temperature at a node, and T_{air} is the temperature of air in the room. The temperature of the atmosphere and the underlying substrate were assumed to be 298 K.

The Q_{RF} term indicates the volumetric heat source due to the RF field. We describe this field using a simple approximation: If a given location (x, z) is within a user specified range of the RF field source, then this term is turned on. Just as the RF power was modulated in the lab experiment to keep the maximum temperature of the resin in the range of 130-150 °C, the model similarly employs proportional control of the Q_{RF} term with a steady-state gain of 1 based on the maximum temperature of the resin reservoir.

The boundary conditions of the system are as follows: the system experiences heat loss via convection through both the sides and the top (in the positive and negative x-direction, and in the positive z-direction) and conduction to a glass substrate through the bottom (in the negative z-direction). These conditions are valid for a structure like a rectangular wall that encompasses the defined system, but in order

to print complex shapes like a pyramid or turret, the simulation needs to be able to identify when and where the resin is deposited. At time = 0 seconds, the system is composed of air, and the simulation uses an external function to calculate the time when the resin is deposited, and the (x,z) location where the resin is deposited. This computed time is used to distinguish the locations where the system is composed of air and epoxy by applying **Equations 1-3** only in the spots where the resin is deposited to model the printing and curing processes.

For printing cylindrical structures, the boundary conditions mentioned above were changed to periodic boundary conditions. The printed structure can be curved to model a three-dimensional open cylindrical structure.

Characterization

Dynamic Mechanical Analysis. Dynamic Mechanical Analysis (DMA) was performed using a TA Instruments DMA 850 to measure and compare the thermo-mechanical properties of RF cured and conventionally cured samples. Moduli change as a function of temperature was observed using a 35 mm dual cantilever test for both samples with a temperature ramp from 35 °C to 120 °C, at a rate of 3 °C/min. A strain of 0.04 % and frequency of 1 Hz was set for all the tests.

Scanning Electron Microscopy. Cross-sectional morphology of samples cured using RF heating and conventional oven heating were observed using an FEI Quanta 600 FE-SEM.

Mechanical Testing. Longitudinal tensile testing was conducted on ASTM D638 type IV tensile bars cured using RF heating and conventional ovens using an Instron load frame with a 30 kN load cell. The displacement rate was set to be 2 mm/min. The raw data of Load, F [N] vs Displacement, d [mm] was converted to Stress σ [N/m^2] vs Strain ε [%], and ultimate tensile strength was compared for tensile bars made using either curing method. Five samples made using either manufacturing method were tested and compared.

Results and Discussion

We first discuss rheology and RF heating results for varied CNT loadings to determine the ideal filler loading for our process. Next, we discuss printing results and demonstrate the ability of our process to print high-resolution complex shapes. After that, we discuss the characterization results of our printed parts and compare them to parts cured using conventional methods. Finally, we discuss simulation results, which assess how certain print parameters affect the properties of the final part and the ability of our process to print other complex shapes.

Ink properties

The resin needs to meet certain rheological requirements to be an effective ink for Direct Ink Write printing. The DIW printing process can be divided into four major sections: (1) static (rest) state inside the print head; (2) shear flow inside the nozzle; (3) high shear extrusion inside the nozzle and (4) static (rest) state on the print bed. An ideal DIW resin ink should be a stable viscoelastic solid at rest, flow when subjected to shear stress, and recover its properties once high shear stress is removed. The rheological properties of the resin with different CNT loadings were investigated to determine a suitable candidate resin for DIW printing. **Figure 2** shows that there is an increase in yield stress of CNT-filled resin with an increase in CNT loading. A very low yield stress (~1 Pa) will mean that the uncured resin will collapse without any resistance to deformation; however, a very high yield stress (>100 Pa) is also not preferable as it cannot be easily extruded from the printer nozzle (**Figure S3**).

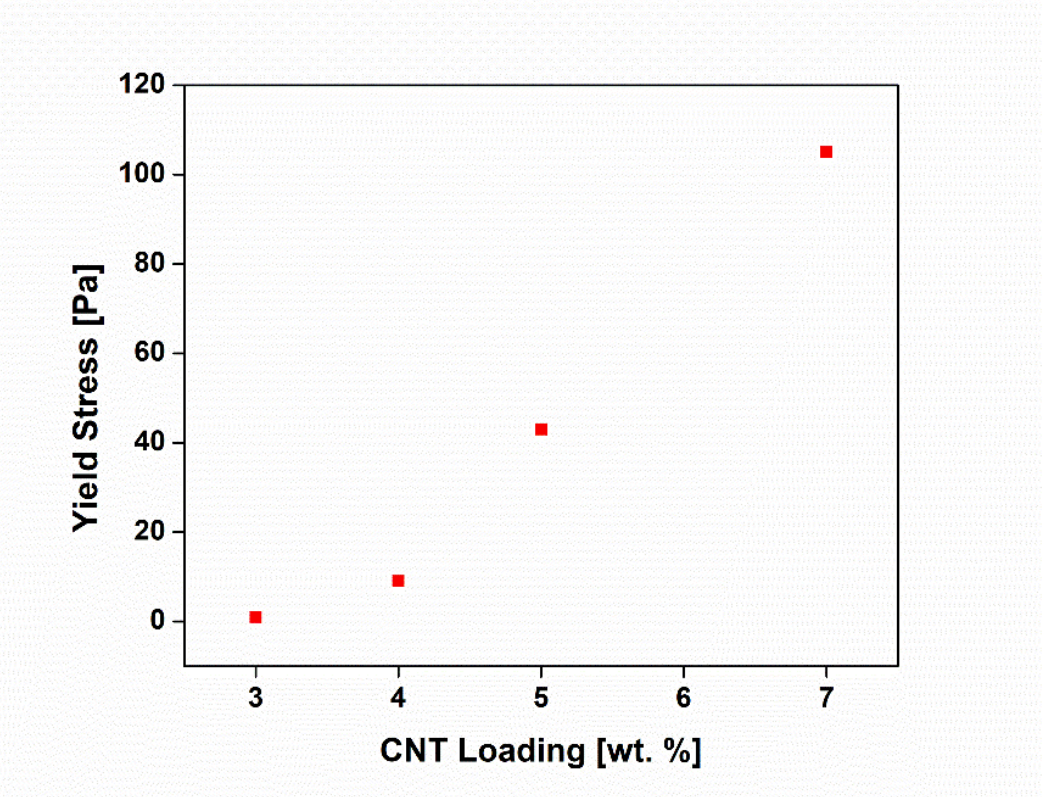

Figure 2: Yield stress obtained from oscillatory stress sweeps as a function of CNT loading in uncured resin.

Next, the storage modulus (G') value of the resin before and after the high shear process was measured (**Figure 3**). We see an increase in modulus value and the recovery of the resin viscosity after high shear with an increase in CNT loading. In a printing process, after the high shear extrusion from nozzle, a high storage modulus of the resin at low frequencies represents rigidity and shape retention of the printed form.

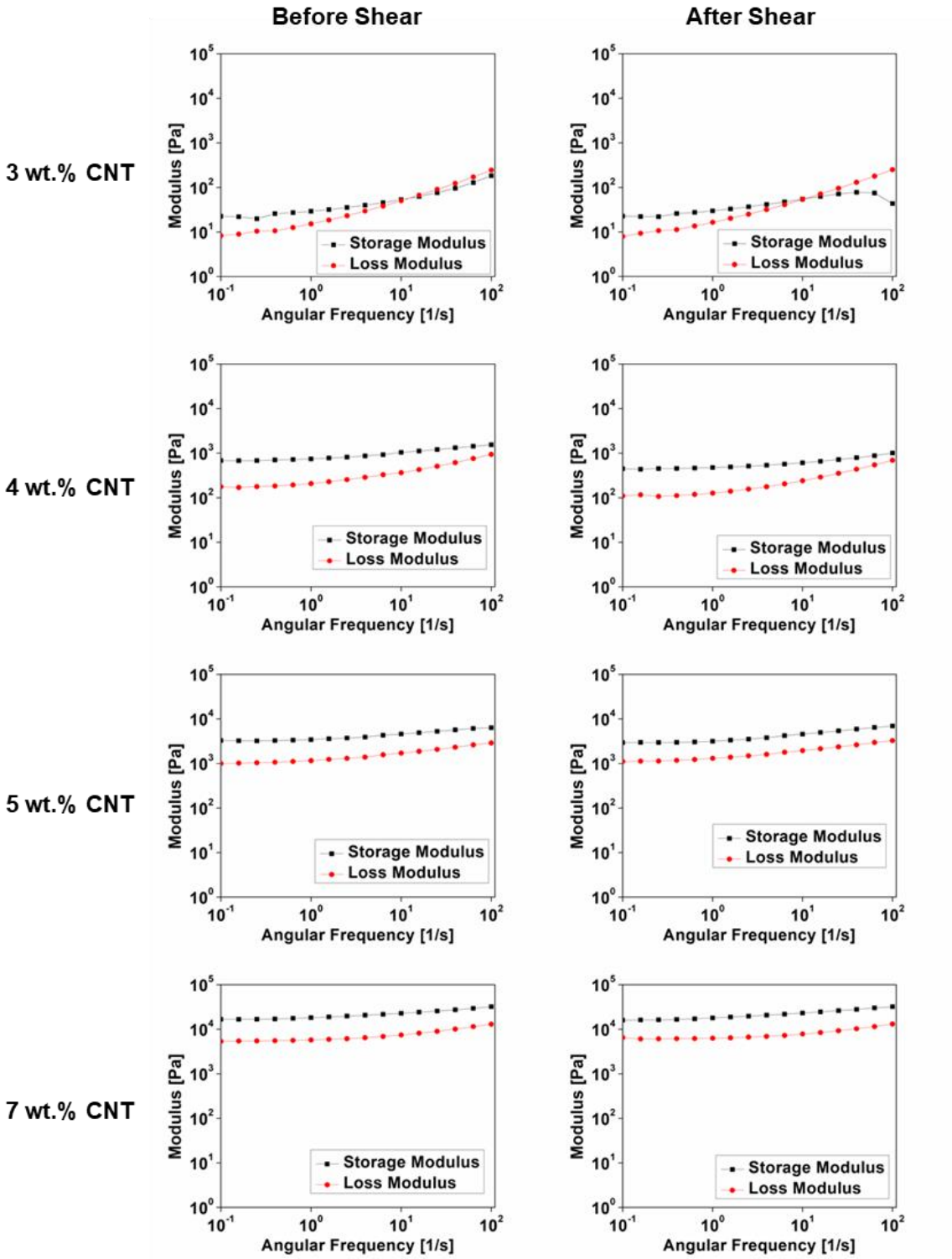

Figure 3: Dynamic frequency sweep plots of uncured CNT-loaded resin at different CNT loadings, before and after subjecting to high shear. The storage modulus of the resin before and after high shear was monitored to determine shape retention of the printed part.

Finally, a three-interval thixotropy test (3ITT) was performed to determine the recovery in viscosity of the resin after exposing it to high shear; the results show that the percentage of viscosity recovered

increased with CNT loading (**Figure 4**). A high viscosity post shear is preferred because it enables the printed part to hold its shape and maintain resolution.

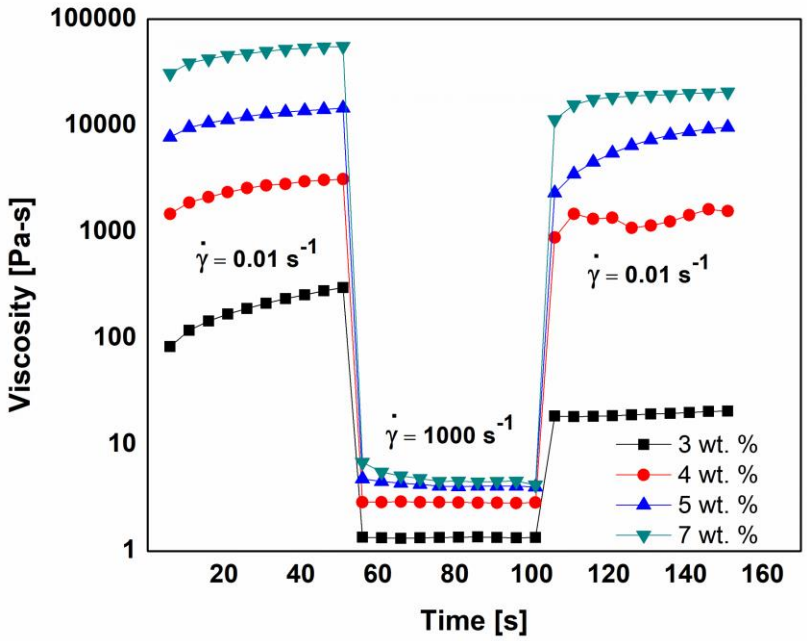

Figure 4: Three interval steady-shear thixotropy results for varied CNT loadings in uncured resin. The three regions in this test are as follows: an initial rest period (0.01 s^{-1}), a high shear-rate step (1000 s^{-1}), and the recovery period (0.01 s^{-1}).

The sample with 3 wt.% CNT loading showed low yield stress and poor recovery of storage modulus and viscosity modulus post high shear, making this resin fairly unsuitable for printing. Samples with 5 wt.% and 7 wt.% CNT loading showed high yield stress and good recovery of storage modulus and viscosity values; however, in order to demonstrate the ability of our system to print relatively low viscosity inks with high resolution, we chose 4 wt.% as our candidate resin. The resin with a loading of 4 wt.% had workable yield stress and showed good recovery of G' and viscosity values post high shear.

Ink heating properties

The rate of heating was measured for epoxy-CNT samples at different CNT loadings when the samples were exposed to radio-frequency fields across a frequency range of 1-200 MHz (**Figure S4**). The results show a rise in RF response with an increase in CNT loading; this can be quantified by the instantaneous heating rate observed for each sample when exposed to RF. The plot of the heating rate as a function of CNT loadings is shown in **Figure 5**. While 3 wt.% shows very low RF response, the other loadings (4, 5, and 7 wt.%) show rapid heating rates (approaching > 100 °C in ~15 seconds at 1 W), which is required for our layer-by-layer RF heating process. Thus, resin with 4 wt.% loading of CNTs is chosen for our printing experiments, as it showed desired rheological properties and RF heating response.

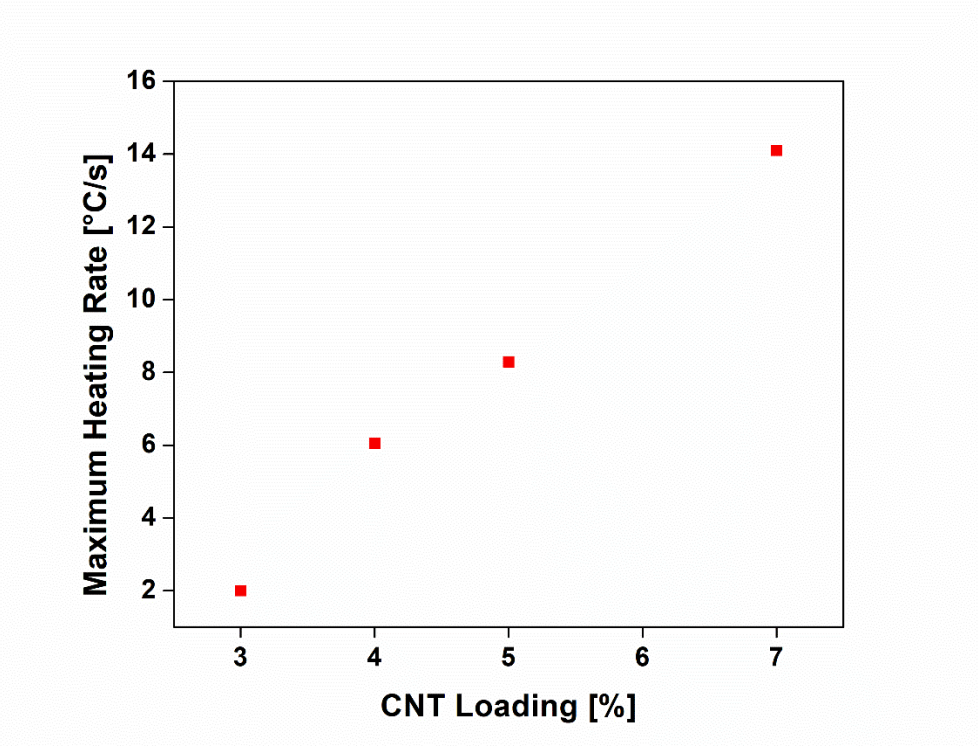

Figure 5: Maximum heating rate measured as a function of CNT loading in uncured resin. The CNT-filled resin was exposed to Radio-frequency fields at a constant power of 1 watt, with frequencies ranging from 1-200 MHz.

Printing Results

Here, we demonstrate our new method for DIW printing and RF curing of thermosetting epoxies using a print-and-cure cycle. We first compared the print quality, shape retention, and the ability of the structure to hold the weight of subsequent printed layers with and without partial RF curing after each layer was printed. **Figure 6a** shows the ideal print shape, and we compare the images in **Figures 6b-c** against this ideal shape. The results in **Figure 6b and 6c** show a printed wall without RF heating after each layer and with RF heating after each layer, respectively. We observed that the structure collapsed after 5 printed layers when it was not partially cured using RF heating. On the other hand, the printed structure that was RF heated after each layer was able to maintain height without collapsing for 8 layers. These results demonstrate that partial curing using RF heating allows the structure to support the weight of subsequent layers. **Figure 6d** shows a wall printed using DIW and RF heating of a sample with 10 wt.% CNT; this shows that our method can be extended to resins with high filler loadings.

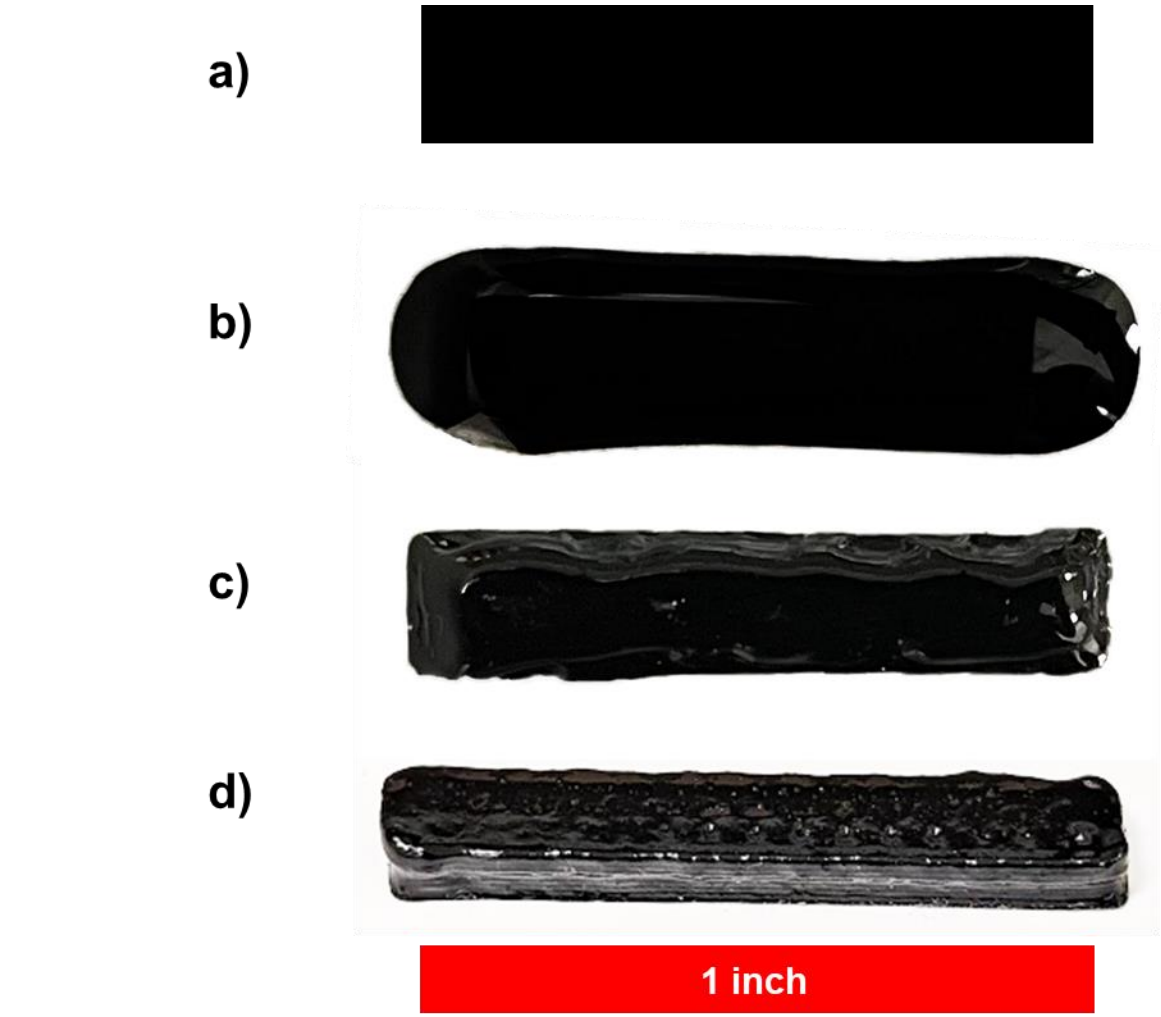

Figure 6: Walls printed using DIW and 4 wt.% CNT resin: (a) A top-down view of the CAD file showing the ideal wall shape. (b) Wall printed without RF cure, which caused structural collapse after 5 layers. (c) Wall printed with RF partial cure after each layer, no structural collapse at 8 layers. (d) Wall printed using 10 wt. % CNT resin with RF cure, showing RF and viscosifying techniques can easily be combined.

We printed various complex shapes to demonstrate different aspects of print quality. The first shape is a gear with a height of ~0.2 mm (**Figure 7a**). This gear print shows that multi-layered complex structures can be successfully manufactured using this methodology. Next, we printed a single-trace hexagon (**Figure 7b**). The sharp corners in **Figure 7b** indicate that the print-and-cure cycle followed after each printed layer allows for the printed part to maintain its resolution without relying on long curing schedules or high viscosity ink systems.

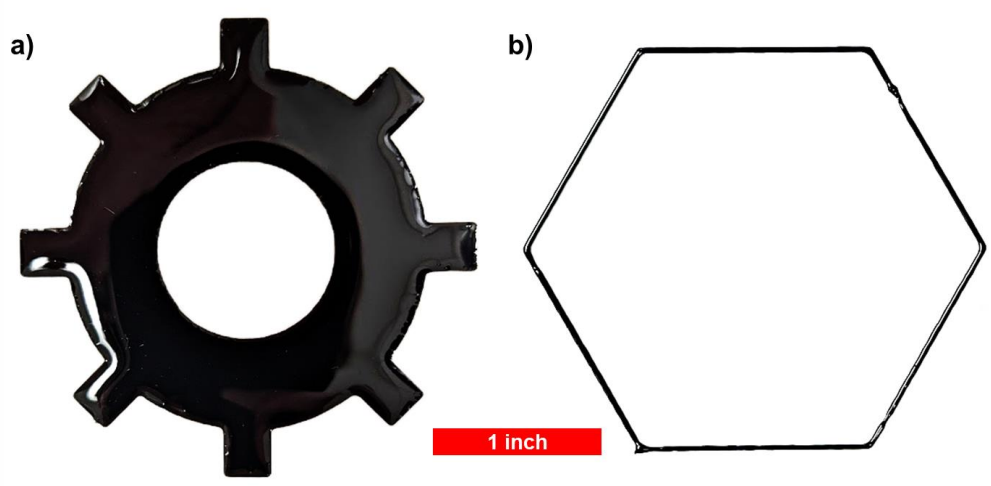

Figure 7: Complex shapes manufactured using direct-ink write printing and RF heating and curing: (a) A complex gear print, (b) single-trace hexagon.

Characterization

Dynamic Mechanical Analysis (DMA) results show that the elastic moduli of a sample manufactured conventionally (oven cured) is similar to a sample manufactured using DIW printing and RF heating (**Figure 8**). Both samples were cured at the same temperature (150 °C) and residence time (5 minutes). Furthermore, the glass transition temperature observed for the RF cured sample (87.5 °C) and the conventionally cured sample (79.3 °C) is also similar, which demonstrates that the samples printed using RF curing method have similar thermal and mechanical properties compared to the conventional oven-cured samples.

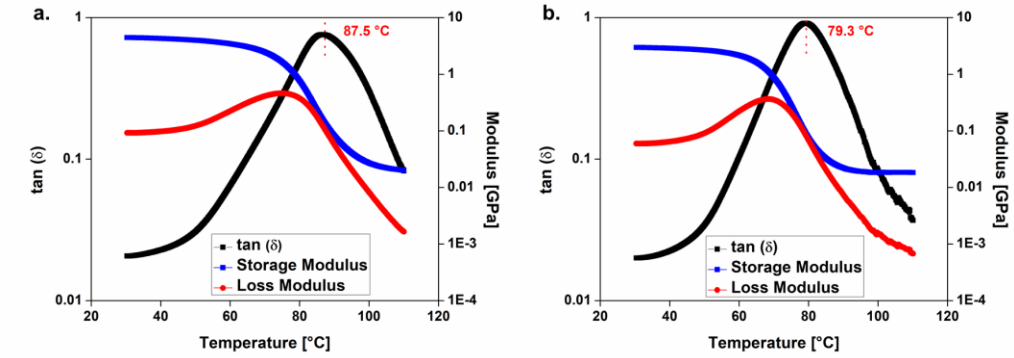

Figure 8: Dynamic Mechanical Analysis (DMA) plots for samples fabricated using (a) DIW printing + RF curing, and (b) oven curing in a mold. A 35-mm dual cantilever beam procedure was followed at a frequency of 1 Hz.

The cross-section of samples manufactured using RF heating or conventional curing were observed using SEM (**Figure 9**). RF heating is a volumetric heating method which means that the sample heats from inside-to-outside, eliminating trapped air bubbles, and resulting in a uniform morphology (**Figure 9a-b**). Here, distinct printed layers are not visible in the cross-sectional morphology; this shows that the print and cure cycle using RF heating allows for sufficient inter-layer adhesion. Comparing these results to conventional curing, which employs convective heating, the outer layer of the print cures first, trapping air bubbles inside the final part, and leading to voids in the sample and decreased mechanical strength (**Figure**

9c-d). This is consistent with our prior work, which involved manufacturing of nanocomposites using selective RF heating and curing[35].

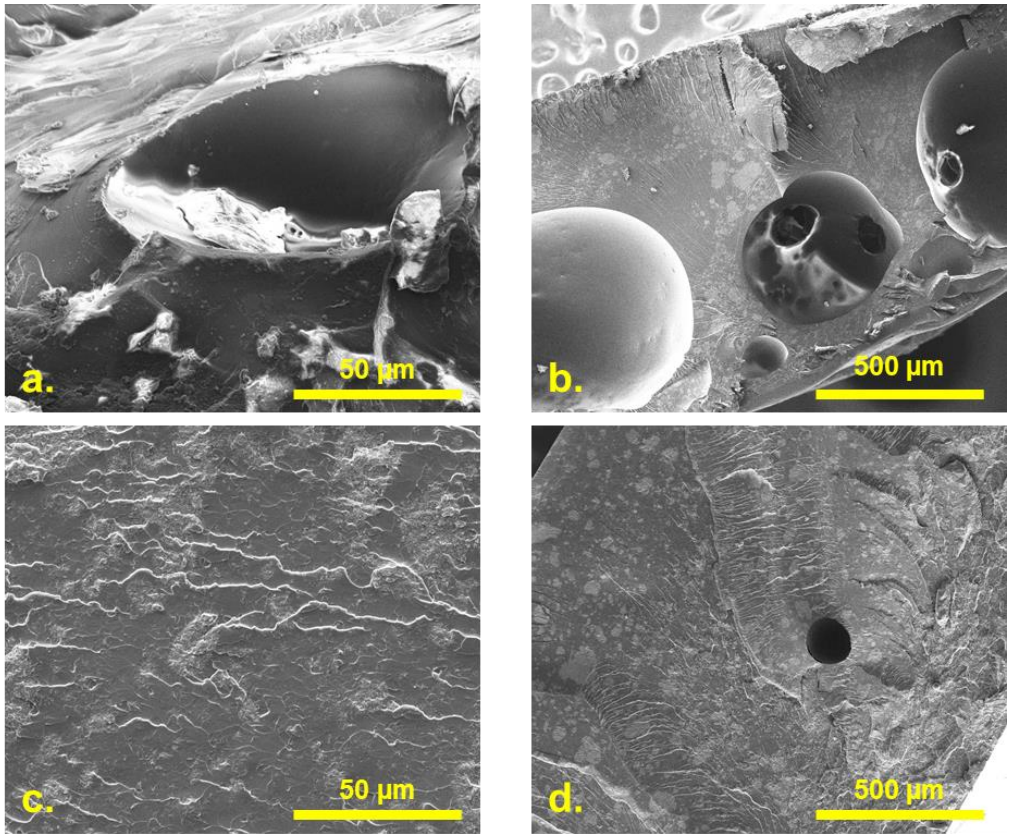

Figure 9: Scanning Electron Microscopy (SEM) images of sample cross sections. CNT-filled epoxy samples were manufactured using (a-b) conventional oven curing in a mold and (c-d) DIW printing and RF heating.

The mechanical properties of ASTM D638 Type IV tensile bars were measured and compared for samples manufactured via two methods: (i) Direct Ink Writing with RF heating, and (ii) conventional oven curing in a mold. The DIW printed samples which were cured using RF heating had a tensile strength of ~23.1 MPa, while conventionally made samples yielded a tensile strength of ~18.6 MPa (**Figure 10**). The slightly higher tensile strength of RF cured samples could be because volumetrically cured samples have a lower void fraction compared to samples cured using convective heating (oven curing).

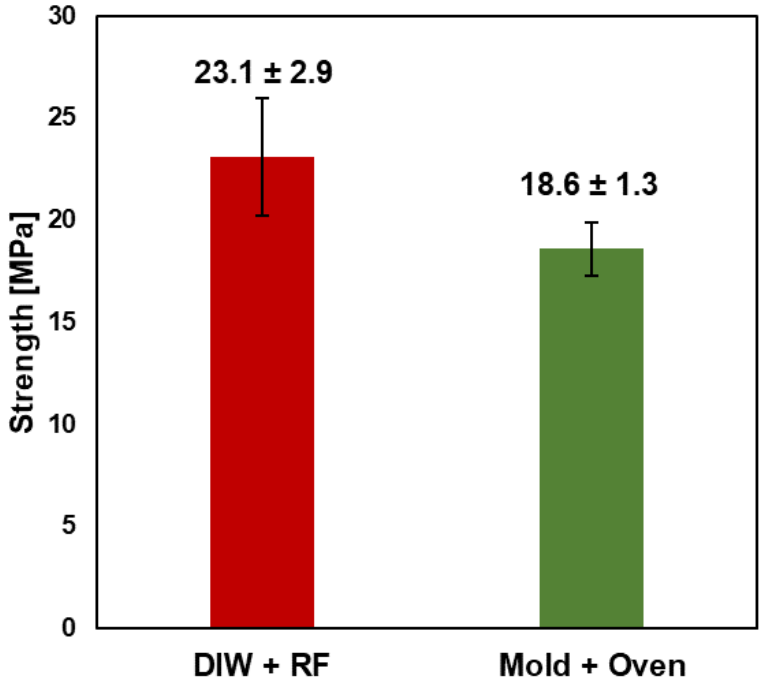

Figure 10: Ultimate tensile strength values for ASTM D638 Type IV tensile bars cured using DIW Printing + RF heating and oven curing in a mold.

Simulation Results

We used finite differences to simulate the spatiotemporal kinetics of a resin reservoir exposed to a moving heat source to print complex structures. The simulation computes the temperature and the percent of epoxy cured (referred to as conversion, or X) changing with time at each point in space. The localized RF heating was mimicked using a localized heat source with a specified path in space and time. The purpose of the following simulations is to demonstrate the potential of this method as well as to help optimize the printing and curing parameters for manufacturing thermosetting resin parts using DIW printing and RF heating.

First, we used the model to demonstrate the DIW printing, RF heating, and curing of thermosetting epoxy loaded with 4 wt. % CNT. For this simulation, temperature and conversion are computed as a function of time for each time step. The input path, comprised of (x,z) locations, specifies the movement of print-head and heat source to form a wall structure with a layer height of 0.001 m. The temperature of the heat source in the simulation was modulated to be within 140-150 °C. The print speed was calculated such that each spot is approximately 60% cured at 140-150 °C. The resulting temperature and conversion are depicted as a function of space at three different times in **Figure 11**.

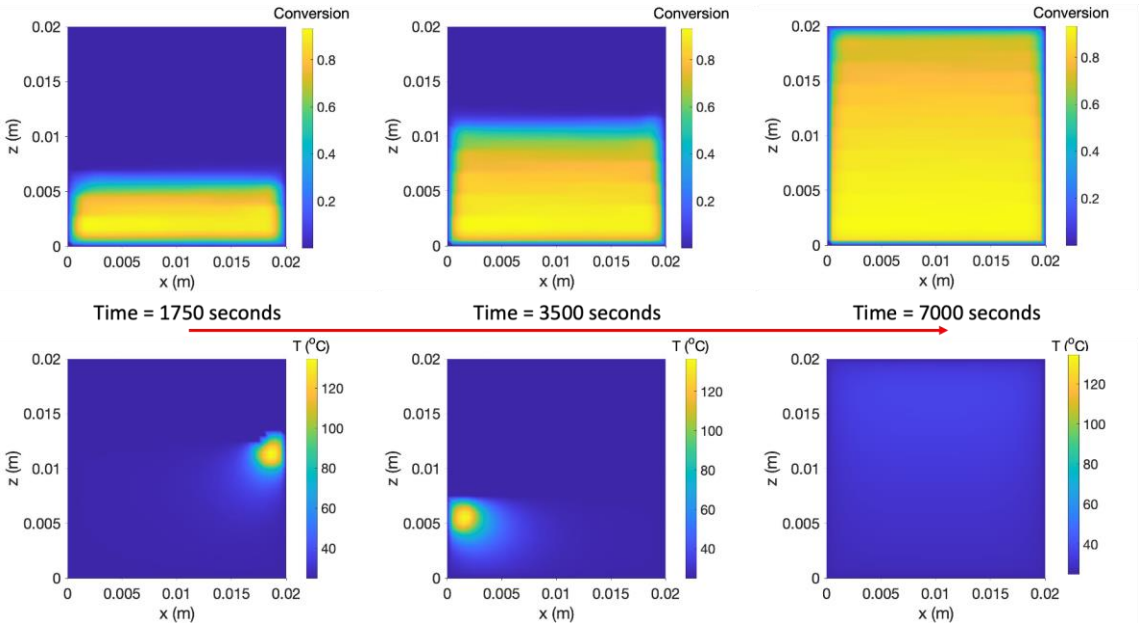

Figure 11: Surface plot of temperature and conversion of a wall changing with time (t = 1750 seconds, 3500 seconds, 7000 seconds) and space.

Similarly, another wall structure was simulated with a layer height of 0.002 m; all other input parameters remain the same as in the previous simulation. **Figure 12** shows a comparison of conversion at the final time of the two wall structures. The results in Figure **12** indicate that the layer height can have a significant impact on how much each layer of the structure cures, and the maximum achievable structure height. The lower conversion observed with a larger layer height in **Figure 12b** could result in the printed structure collapsing at a shorter height. This means that, in addition to the rheological properties of the resin, the printing parameters themselves could affect print resolution and end-use properties.

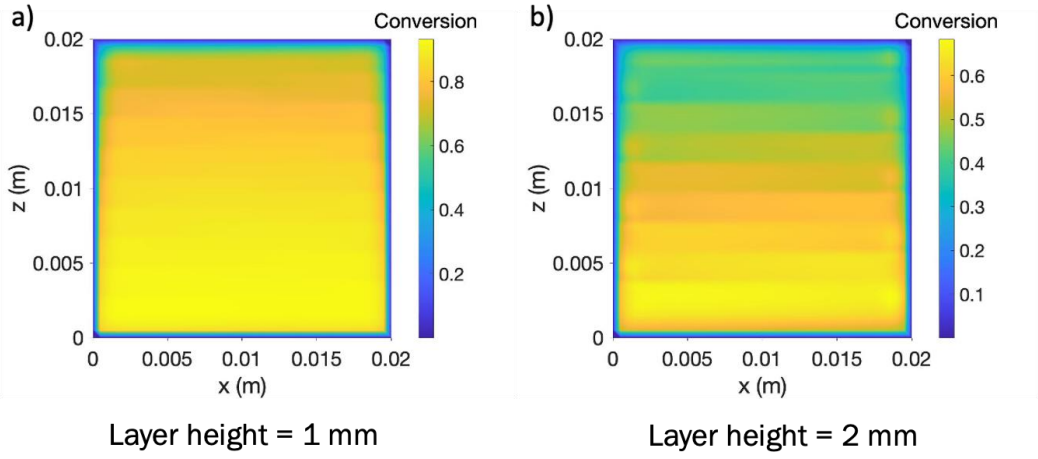

Figure 12: Surface plot of conversion of a wall as a function of space at the final time. The structures have a layer height of (a) 0.001 m, and (b) 0.002 m. Other parameters like residence time, target temperature, and system parameters remain unchanged.

Next, we show the potential of this method in printing three-dimensional shapes like an open cylinder with a small thickness. This simulation follows the same parameters as the wall in **Figure 11**; however, the boundaries in this simulation are periodic, i.e., continuous in the x-direction, thereby simulating a 3D cylinder via a 2D simulation (neglecting curvature effects). The results in **Figure S5** show

conversion and temperature as a function of space and time at two different time points: the halfway time and the final time. The temperature plot demonstrates periodic boundary conditions by showing the heat transfer from one side to the other when the heat source is at a side boundary. The surface plot of the conversion at the final time was superimposed over a cylindrical structure to provide an illustration of the three-dimensional shape (**Figure 13**).

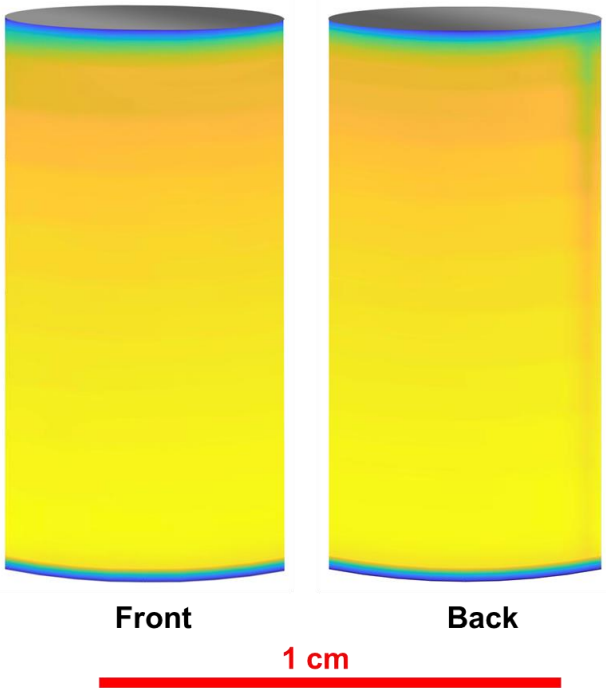

Figure 13: Surface plot of conversion of a cylinder mapped onto a cylindrical surface to show the three-dimensional structure. This figure corresponds to results shown in Figure S5.

We also illustrate how complex shapes like a turret can be printed using our technology**.** The results in **Figure 14a** indicate that complex structures with high resolution are achievable with this technology. Note that the resolution of these results is limited by the simulation mesh size rather than the nozzle size or heat source range. The final cured structure is remarkably similar to the input print path **(Figure 14b**), allowing engineers to produce structures that are similar to an original CAD design.

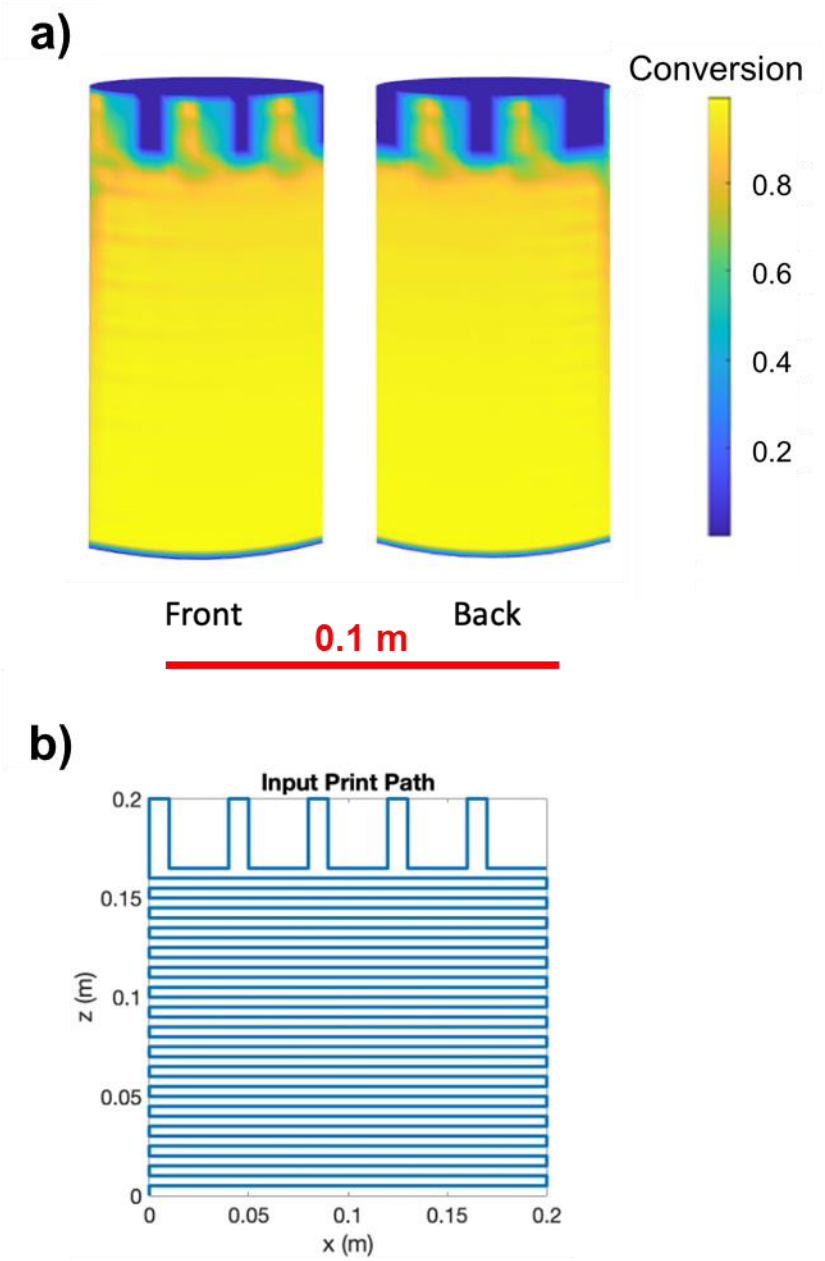

Figure 14: (a) Surface plot of conversion of a turret as a function of space at the end of the simulation, mapped onto a cylindrical surface to show the three-dimensional structure. (b) Plot of the input print path used to simulate the turret.

Conclusions

In this study, we have successfully developed a novel methodology for additive manufacturing of thermoset nanocomposites via Direct Ink Writing coupled with localized, radio-frequency heating. The repeated print-and-cure cycle described in this work allows for the fabrication of multi-layered thermoset parts without relying on any viscosity modifying agents or novel chemistries. Rheological properties and RF response of the resin at different carbon nanotube loadings were analyzed prior to printing in order to determine a carbon nanotube loading suitable for our printing system. Complex shapes with high print resolution were achieved using the proposed methodology. Thermomechanical characterization showed that samples cured using RF heating had comparable storage moduli values when compared to a

conventional, oven-cured sample. Tensile testing yielded better strength values for the RF-cured samples than the oven-cured samples; this could be attributed to the fact that volumetric, RF heating results in a void-free, smooth morphology of the final part, as seen from the cross-sectional SEM images. Simulation results show how certain printing parameters such as layer height affect the final printed structure; further, simulations also show that this additive manufacturing methodology could be further explored for free-form printing of other complex shapes as well. This work establishes localized RF heating and DIW printing as a feasible approach for additive manufacturing of thermoset nanocomposites.

Acknowledgments

The authors acknowledge the Scientific and Technological Research Council of Turkey (TUBITAK) 2219-International Postdoctoral Research Fellowship Program for Turkish Citizens for their sponsorship. The authors also acknowledge A*STAR Graduate Academy - A*STAR International Fellowship Program for their sponsorship. Use of the Texas A&M University Soft Matter Facility (RRID:SCR_022482) for DMA is acknowledged. The authors thank the Materials and Testing Lab at TAMU for their Mechanical Testing setup. The authors thank the Microscopy and Imaging Center at TAMU for SEM. This work was supported by Honeywell Federal Manufacturing & Technologies, LLC, which operates the Kansas City National Security Campus for the United States Department of Energy / National Nuclear Security Administration under Contract Number DE-NA0002839. The authors thank and acknowledge Evan C. Sonnier of TAMU for creating Figures 13 and 14a using our simulation results and Photoshop.

References

1. Johannisson, W.; Zenkert, D.; Lindbergh, G. J. M. M., Model of a structural battery and its potential for system level mass savings. **2019,** *2*, (3), 035002.
2. Pattanaik, A.; Mukherjee, M.; Mishra, S. B., Influence of curing condition on thermo-mechanical properties of fly ash reinforced epoxy composite. *Compos Part B-Eng* **2019,** *176*.
3. Czaderski, C.; Martinelli, E.; Michels, J.; Motavalli, M., Effect of curing conditions on strength development in an epoxy resin for structural strengthening. *Compos Part B-Eng* **2012,** *43*, (2), 398-410.
4. Wu, Q.; Yang, X.; Wan, Q. Q.; Zhao, R. Y.; He, J. Q.; Zhu, J. F., Layer-by-layer assembled nacre-like polyether amine/GO hierarchical structure on carbon fiber surface toward composites with excellent interfacial strength and toughness. *Compos Sci Technol* **2020,** *198*.
5. Sweeney, C. B.; Lackey, B. A.; Pospisil, M. J.; Achee, T. C.; Hicks, V. K.; Moran, A. G.; Teipel, B. R.; Saed, M. A.; Green, M. J., Welding of 3D-printed carbon nanotube-polymer composites by locally induced microwave heating. *Sci Adv* **2017,** *3*, (6).
6. Blok, L. G.; Longana, M. L.; Yu, H.; Woods, B. K. S., An investigation into 3D printing of fibre reinforced thermoplastic composites. *Addit Manuf* **2018,** *22*, 176-186.
7. Sweeney, C. B.; Burnette, M. L.; Pospisil, M. J.; Shah, S. A.; Anas, M.; Teipel, B. R.; Zahner, B. S.; Staack, D.; Green, M. J., Dielectric Barrier Discharge Applicator for Heating Carbon Nanotube-Loaded Interfaces and Enhancing 3D-Printed Bond Strength. *Nano Lett* **2020,** *20*, (4), 2310-2315.
8. Visser, C. W.; Pohl, R.; Sun, C.; Roemer, G. W.; in 't Veld, B. H.; Lohse, D., Toward 3D Printing of Pure Metals by Laser-Induced Forward Transfer. *Adv Mater* **2015,** *27*, (27), 4087-4092.
9. Gibson, M. A.; Mykulowycz, N. M.; Shim, J.; Fontana, R.; Schmitt, P.; Roberts, A.; Ketkaew, J.; Shao, L.; Chen, W.; Bordeenithikasem, P.; Myerberg, J. S.; Fulop, R.; Verminski, M. D.; Sachs, E. M.; Chiang, Y. M.; Schuh, C. A.; Hart, A. J.; Schroers, J., 3D printing metals like thermoplastics: Fused filament fabrication of metallic glasses. *Mater Today* **2018,** *21*, (7), 697-702.
10. Parekh, D. P.; Ladd, C.; Panich, L.; Moussa, K.; Dickey, M. D., 3D printing of liquid metals as fugitive inks for fabrication of 3D microfluidic channels. *Lab Chip* **2016,** *16*, (10), 1812-1820.

11. Srai, J. S.; Kumar, M.; Graham, G.; Phillips, W.; Tooze, J.; Ford, S.; Beecher, P.; Raj, B.; Gregory, M.; Tiwari, M. K.; Ravi, B.; Neely, A.; Shankar, R.; Charnley, F.; Tiwari, A., Distributed manufacturing: scope, challenges and opportunities. *Int J Prod Res* **2016,** *54*, (23), 6917-6935.
12. Zhang, B.; Kowsari, K.; Serjouei, A.; Dunn, M. L.; Ge, Q., Reprocessable thermosets for sustainable three-dimensional printing. *Nat Commun* **2018,** *9*.
13. Tumbleston, J. R.; Shirvanyants, D.; Ermoshkin, N.; Janusziewicz, R.; Johnson, A. R.; Kelly, D.; Chen, K.; Pinschmidt, R.; Rolland, J. P.; Ermoshkin, A.; Samulski, E. T.; DeSimone, J. M., Continuous liquid interface production of 3D objects. *Science* **2015,** *347*, (6228), 1349-1352.
14. Wu, T.; Jiang, P.; Zhang, X. Q.; Guo, Y. X.; Ji, Z. Y.; Jia, X.; Wang, X. L.; Zhou, F.; Liu, W. M., Additively manufacturing high-performance bismaleimide architectures with ultraviolet-assisted direct ink writing. *Mater Design* **2019,** *180*.
15. Wei, L.; Li, J.; Zhang, S.; Li, B.; Liu, Y.; Wang, F.; Dong, S. X., Fabrication of SiOC ceramic with cellular structure via UV-Assisted direct ink writing. *Ceram Int* **2020,** *46*, (3), 3637-3643.
16. Guo, Y. X.; Xu, J. W.; Yan, C. Y.; Chen, Y. Q.; Zhang, X. Q.; Jia, X.; Liu, Y.; Wang, X. L.; Zhou, F., Direct Ink Writing of High Performance Architectured Polyimides with Low Dimensional Shrinkage. *Adv Eng Mater* **2019,** *21*, (5).
17. Tu, R. W.; Sodano, H. A., Additive manufacturing of high-performance vinyl ester resin via direct ink writing with UV-thermal dual curing. *Addit Manuf* **2021,** *46*.
18. Yirmibesoglu, O. D.; Simonsen, L. E.; Manson, R.; Davidson, J.; Healy, K.; Menguc, Y.; Wallin, T., Multi-material direct ink writing of photocurable elastomeric foams. *Commun Mater* **2021,** *2*, (1).
19. Malik, M. S.; Schlogl, S.; Wolfahrt, M.; Sangermano, M., Review on UV-Induced Cationic Frontal Polymerization of Epoxy Monomers. *Polymers-Basel* **2020,** *12*, (9).
20. Robertson, I. D.; Yourdkhani, M.; Centellas, P. J.; Aw, J. E.; Ivanoff, D. G.; Goli, E.; Lloyd, E. M.; Dean, L. M.; Sottos, N. R.; Geubelle, P. H.; Moore, J. S.; White, S. R., Rapid energy-efficient manufacturing of polymers and composites via frontal polymerization. *Nature* **2018,** *557*, (7704), 223-+.
21. Li, L. Y.; Lin, Q. M.; Tang, M.; Duncan, A. J. E.; Ke, C. F., Advanced Polymer Designs for Direct-Ink-Write 3D Printing. *Chem-Eur J* **2019,** *25*, (46), 10768-10781.
22. Mahmoudi, M.; Burlison, S. R.; Moreno, S.; Minary-Jolandan, M., Additive-Free and Support-Free 3D Printing of Thermosetting Polymers with Isotropic Mechanical Properties. *Acs Appl Mater Inter* **2021,** *13*, (4), 5529-5538.
23. Hmeidat, N. S.; Elkins, D. S.; Peter, H. R.; Kumar, V.; Compton, B. G., Processing and mechanical characterization of short carbon fiber-reinforced epoxy composites for material extrusion additive manufacturing. *Compos Part B-Eng* **2021,** *223*.
24. Romberg, S. K.; Islam, M. A.; Hershey, C. J.; DeVinney, M.; Duty, C. E.; Kunc, V.; Compton, B. G., Linking thermoset ink rheology to the stability of 3D-printed structures. *Addit Manuf* **2021,** *37*.
25. Eom, Y.; Kim, F.; Yang, S. E.; Son, J. S.; Chae, H. G., Rheological design of 3D printable all-inorganic inks using BiSbTe-based thermoelectric materials. *J Rheol* **2019,** *63*, (2), 291-304.
26. Hmeidat, N. S.; Pack, R. C.; Talley, S. J.; Moore, R. B.; Compton, B. G., Mechanical anisotropy in polymer composites produced by material extrusion additive manufacturing. *Addit Manuf* **2020,** *34*.
27. Wimmer, M. G.; Compton, B. G., Semi-solid epoxy feedstocks with high glass transition temperature for material extrusion additive manufacturing. *Addit Manuf* **2022,** *54*, 102725.
28. Anas, M.; Zhao, Y.; Saed, M. A.; Ziegler, K. J.; Green, M. J., Radio frequency heating of metallic and semiconducting single-walled carbon nanotubes. *Nanoscale* **2019,** *11*, (19), 9617-9625.
29. Debnath, D.; Zhao, X. F.; Anas, M.; Kulhanek, D. L.; Oh, J. H.; Green, M. J., Radio frequency heating and reduction of Graphene Oxide and Graphene Oxide - Polyvinyl Alcohol Composites. *Carbon* **2020,** *169*, 475-481.
30. Odom, M. G. B.; Sweeney, C. B.; Parviz, D.; Sill, L. P.; Saed, M. A.; Green, M. J., Rapid curing and additive manufacturing of thermoset systems using scanning microwave heating of carbon nanotube/epoxy composites. *Carbon* **2017,** *120*, 447-453.

31. Patil, N.; Zhao, X. F.; Mishra, N. K.; Saed, M. A.; Radovic, M.; Green, M. J., Rapid Heating of Silicon Carbide Fibers under Radio Frequency Fields and Application in Curing Preceramic Polymer Composites. *Acs Appl Mater Inter* **2019,** *11*, (49), 46132-46139.
32. Sweeney, C. B.; Moran, A. G.; Gruener, J. T.; Strasser, A. M.; Pospisil, M. J.; Saed, M. A.; Green, M. J., Radio Frequency Heating of Carbon Nanotube Composite Materials. *Acs Appl Mater Inter* **2018,** *10*, (32), 27252-27259.
33. Vashisth, A.; Healey, R. E.; Pospisil, M. J.; Oh, J. H.; Green, M. J., Continuous processing of pre-pregs using radio frequency heating. *Compos Sci Technol* **2020,** *195*.
34. Vashisth, A.; Upama, S. T.; Anas, M.; Oh, J. H.; Patil, N.; Green, M. J., Radio frequency heating and material processing using carbon susceptors. *Nanoscale Adv* **2021,** *3*, (18), 5255-5264.
35. Sarmah, A.; Desai, S. K.; Tezel, G. B.; Vashisth, A.; Mustafa, M. M.; Arole, K.; Crowley, A. G.; Green, M. J., Rapid Manufacturing via Selective Radio-Frequency Heating and Curing of Thermosetting Resins. *Adv Eng Mater* **2022**.
36. Tezel, G. B.; Sarmah, A.; Desai, S.; Vashisth, A.; Green, M. J., Kinetics of carbon nanotube-loaded epoxy curing: Rheometry, differential scanning calorimetry, and radio frequency heating. *Carbon* **2021,** *175*, 1-10.

Additive Manufacturing of Thermosetting Resins via Direct Ink Writing and Radio-Frequency Heating and Curing

Anubhav Sarmah[a,1], Suchi K. Desai[a,1], Ava G. Crowley[a], Gabriel C. Zolton[a], Guler Bengusu Tezel[a,b], Ethan M. Harkin[a], Thang Q. Tran[a,c], Kailash Arole[d], Micah J. Green[a,d,*]

[a] Artie McFerrin Department of Chemical Engineering, Texas A&M University, College Station, TX, 77843 USA

[b] Chemical Engineering Department, Bolu Abant Izzet Baysal University, Bolu, 14030 Turkey

[c] Singapore Institute of Manufacturing Technology, 73 Nanyang Drive, 637662, Singapore

[d] Department of Materials Science and Engineering, Texas A&M University, College Station, TX, 77843, USA

*Corresponding authors: E-mail: micah.green@tamu.edu (Micah J. Green)

Supplementary Information

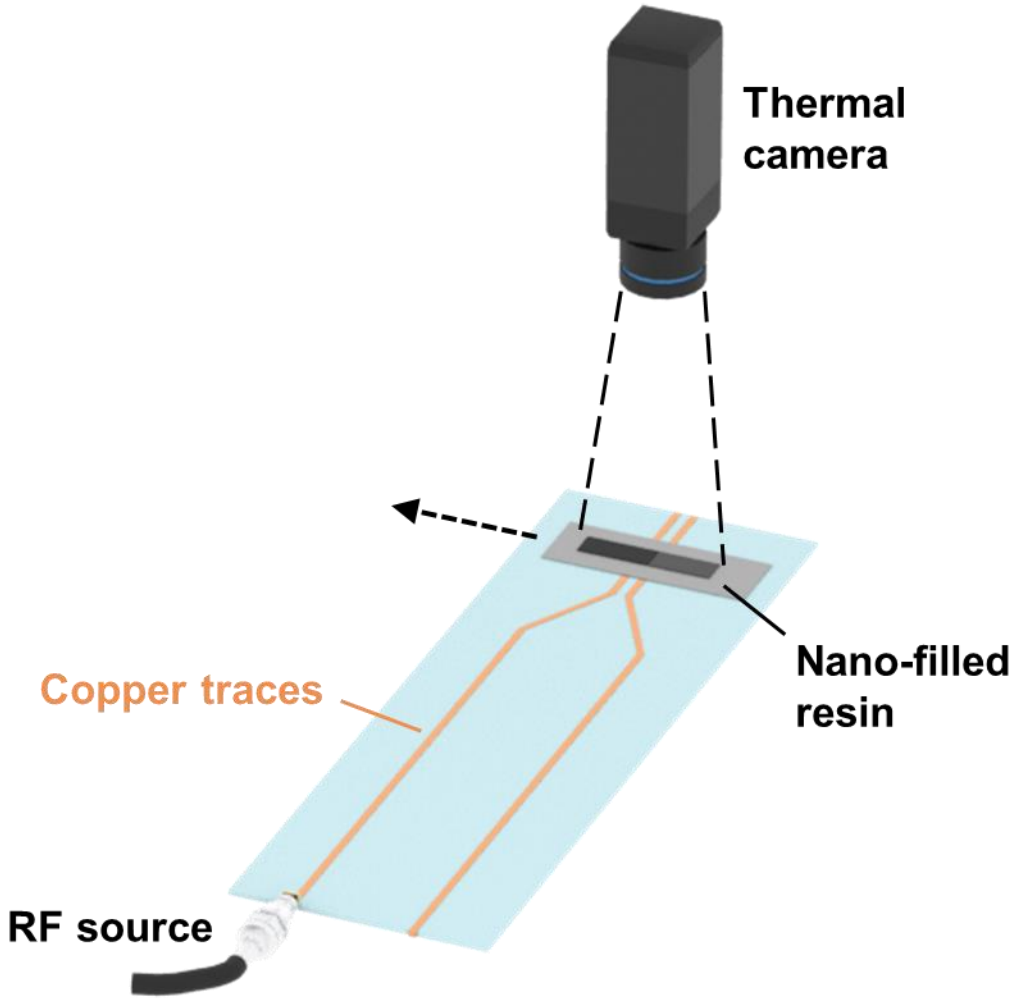

Figure S1: Schematic of fringing field RF applicator for localized heating and curing of DIW printed CNT-filled resin.

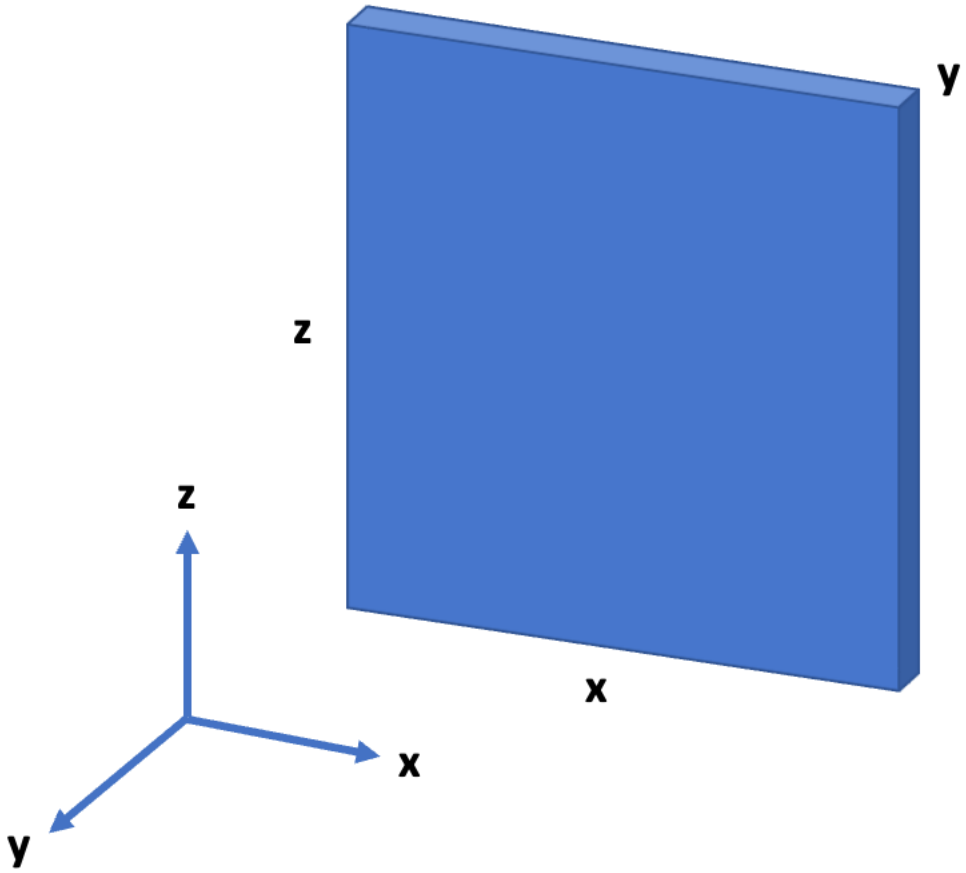

Figure S2: Schematic of simulation system. A two-dimensional (x-z) system with thermal transport (Q_{ext}) in the y-direction.

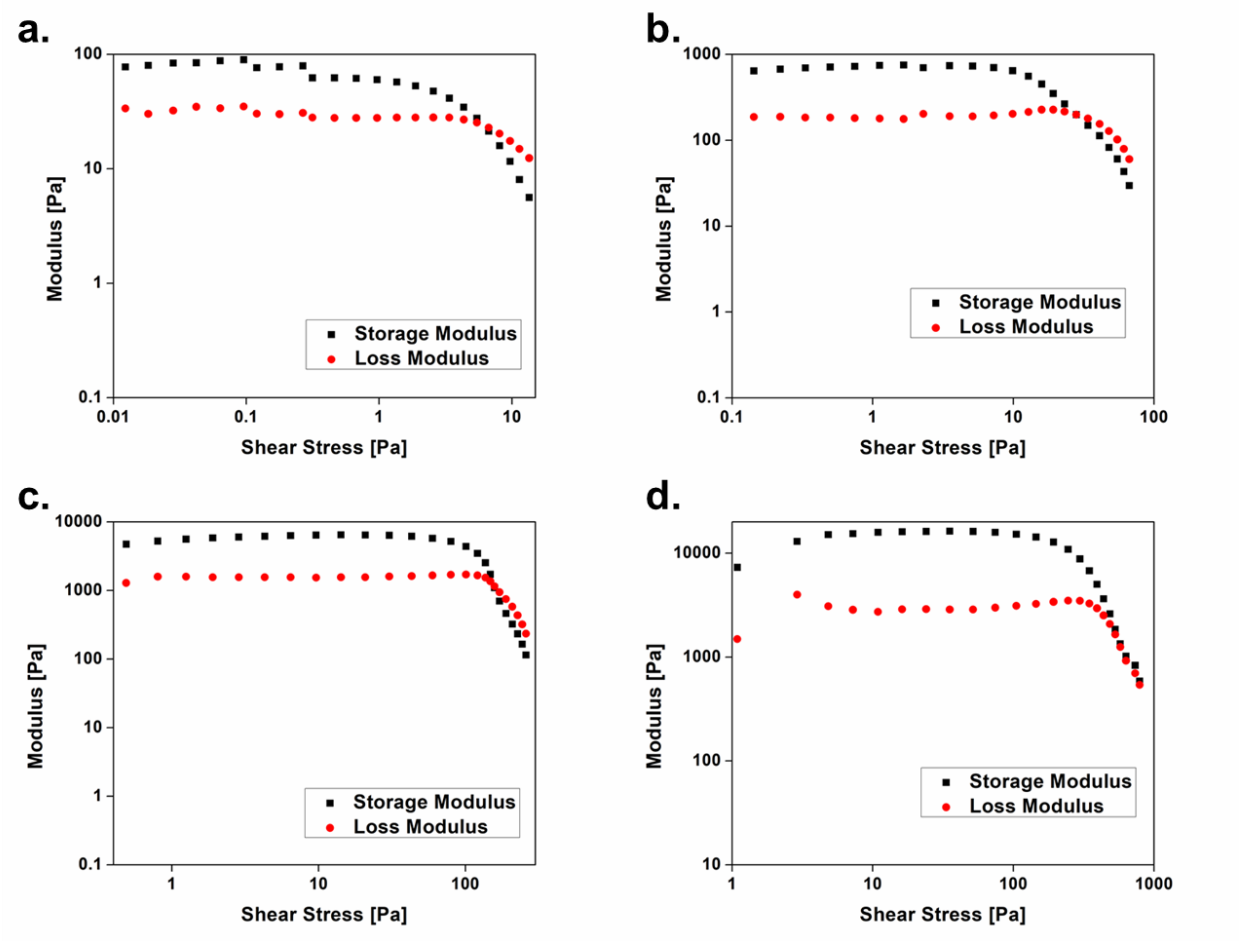

Figure S3: Stress sweep curves for uncured CNT-loaded resin with loading (a) 3 wt.%, (b) 4 wt.%, (c) 5 wt.%, and (d) 7 wt.%.

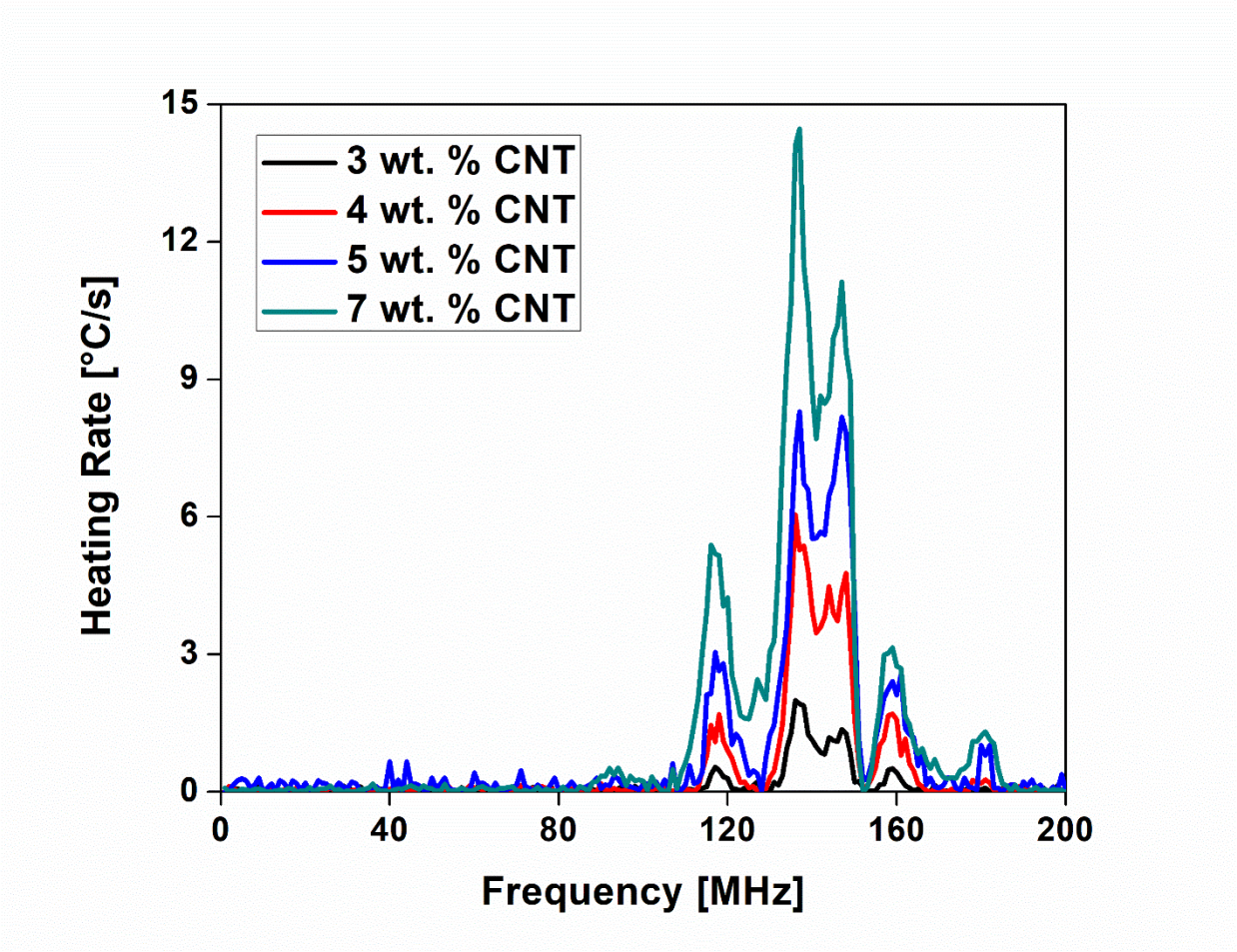

Figure S4: Rate of heating observed across a frequency range of 1-200 MHz at a power of 1 W for CNT-filled resin with loadings of 3, 4, 5 and 7 wt.%.

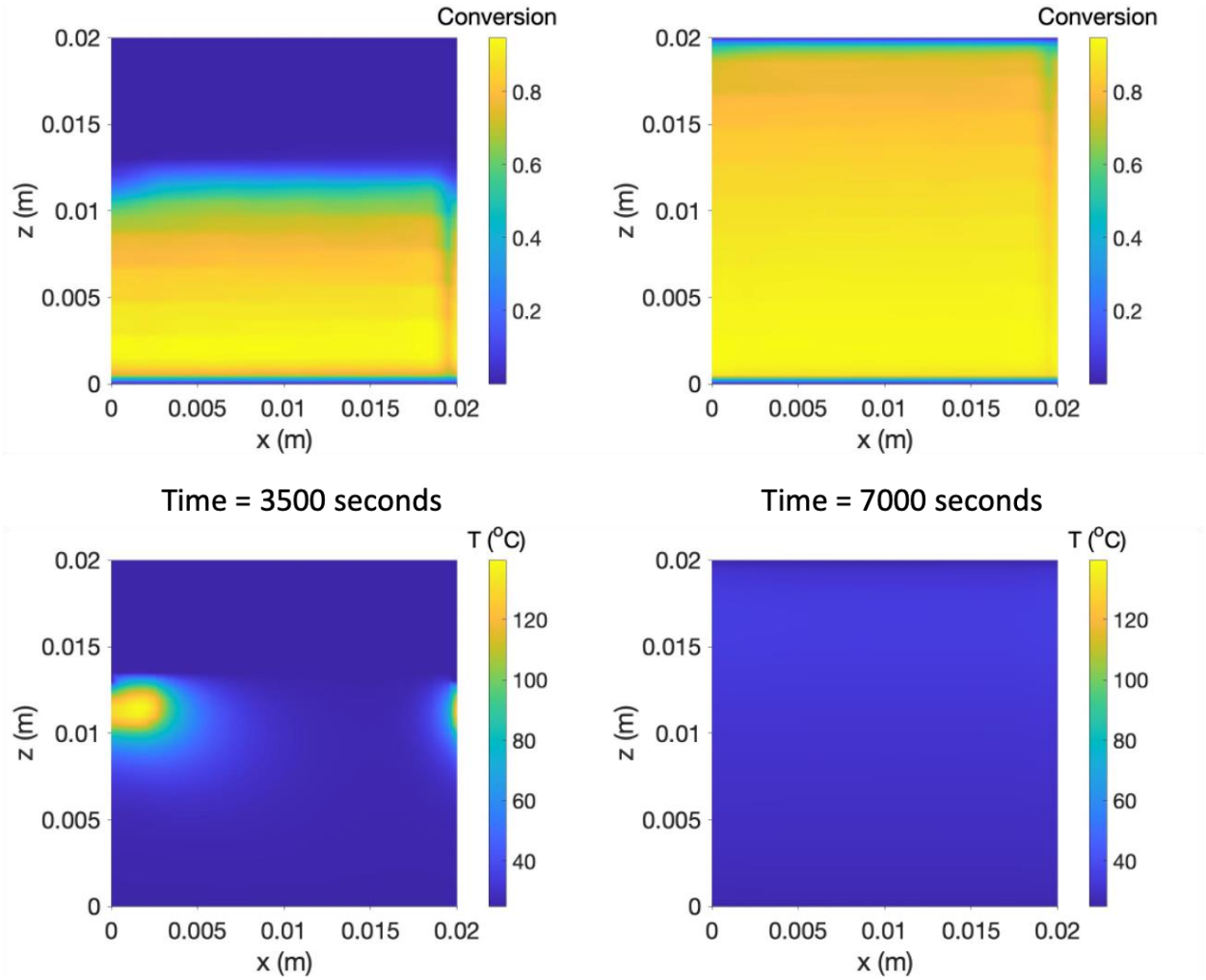

Figure S5: (a) Surface plot of conversion of a cylinder as a function of space at final time, and (b) surface plot of temperature of a cylinder as a function of space at halfway time.